Lithium Elemental Abundance Determination for 4MOST

Emma Solly

Division of Astrophysics
Department of Physics

LUND
UNIVERSITY

2025–EXA244

Degree project of 15 higher education credits
June 2025

Supervisor: Ross Church

Division of Astrophysics
Department of Physics
Box 118
SE-221 00 Lund
Sweden

Abstract

Stellar lithium abundances can help answer multiple unanswered questions within modern astrophysics. Lithium is fragile in comparison to other elements found in stellar atmospheres. Consequently, its abundance within the stellar atmosphere is depleted by different processes. Studying these lithium abundances gives insight into the evolution of the stars and the processes within their interiors. The main aim of this thesis was to develop a method for calculating lithium abundances, given spectra measured by the 4-metre Multi-Object Spectroscopic Telescope (4MOST); a fibre-fed spectrograph which is to begin its operation in 2026. Our method was developed on high resolution synthetic 4MOST spectra with a signal to noise ratio of 1000, and then applied to spectra with a lower signal to noise ratio of 100. In order to calculate the abundance of lithium, the equivalent width of the Li I resonance doublet at 6707.814 Å was first calculated. This line is heavily blended with absorption lines from other elements, including iron, in spectra with sufficient metallicity. In order to calculate the equivalent width of the Li I line in these cases, we assumed that the width of the spectral lines is constant in a wavelength region of 6695 - 6720 Å. Applying a Gaussian fit to unblended lines in this region allowed for measuring this width. A second fit, made to a narrower region across the blended line, was used to obtain the amplitude of the Li I line. The width and amplitude were then used to calculate the equivalent width.

For cases where fewer than three unblended lines were detected in the region around the Li I line, a Gaussian fit was made directly to it. Implemented conditions were used to identify successful, as well as unsuccessful, fits. Determining appropriate conditions for filtering the fits was non-trivial. However, multiple sources of unsuccessful fits were identified.

The curve of growth was used to obtain a lithium abundance from an equivalent width and effective temperature. The dependence on the effective temperature was observed to be significant and so the lithium abundance needed to be calculated as a function of it. The method was applied to 12704 spectra with signal to noise ratio of 100. Out of these, 2775 spectra yielded fits that passed all steps of the filtering process. 4MOST requires the recovered lithium abundance to not vary with more than 0.2 dex from the input lithium abundance. This was achieved for 2000 of the spectra to which successful fits were considered to have been made. A secondary aim of the thesis was to compare our results to those given by the 4MOST pipeline. While a direct comparison could not be made, it seems that the results of our method are comparable to the ones given by the pipeline. Our method has the advantage that it was able to identify cases where a reliable determination of the lithium abundance could not be made.

Popular science introduction

Twinkle twinkle little stars, how I wonder what your lithium abundances are... That is of course not how the song goes. However, this version might be more relatable to an astrophysicist who already knows quite a bit about what the star on the night sky is, but not as much about its evolution. Astronomers have studied the night sky for centuries and have gained insight about the objects adorning it. This has been done by observing the objects' movement and light. Planets were distinguished from stars by their relatively high velocities across the sky and their steady, non-twinkling light. Modern astrophysicists also rely upon the light and dynamics to draw conclusions about the observed objects. Today, techniques such as spectroscopy and photometry are used to study the light in detail.

Radiation produced in the core of a star is absorbed by atoms and molecules in its atmosphere, and then emitted again in random directions. This absorption gives absorption lines at specific wavelengths in the light spectrum that is observed. The wavelengths correspond to a certain energy of the photons, given by a specific energy level separation within an atom or molecule. This gives astrophysicists information about what elements are present in the stellar atmosphere. The strength of the absorption lines is affected by how much absorption has taken place, which in turn is dependent on the amount of the corresponding absorbers. The abundance of a certain element in the stellar atmosphere can therefore be derived from studying the strength of an absorption line that has been caused by atoms of that element.

This process is unfortunately not so straight forward, seeing as one cannot directly read the abundance from the spectrum. The strength of the absorption lines is affected by multiple stellar parameters, not only the abundance of the absorbers. They can also be heavily blended, meaning that the lines are too close in wavelength to distinguish between them. They are instead observed as one line. In this project the element of interest is lithium, which has an absorption line at the wavelength 670.781 nm. Some heavier elements, including iron, give absorption lines close to this wavelength. This results in the lithium line being blended in the spectra from most stars with heavier elements present in their atmospheres. The method developed in this project addresses this issue by assuming that the width of the absorption lines is constant in a region around the lithium line. This width is derived from non-blended lines in the region and the calculation of the strength of the lithium line is simplified, seeing as one now only needs to determine the depth of it via a fit to the blended line.

The aim of this project is to determine the lithium abundance of stars observed with 4MOST, which is an instrument that will observe around 2400 objects on the sky at one time and is estimated to collect tens of millions of spectra. The reason why the lithium abundance is of interest is that lithium is fragile. It is destroyed at temperatures above 2.5 MK, which is low in the context of stellar interiors. Certain events in a star's life have been found to cause a decrease in the abundance of lithium. The abundance can therefore give insight into the evolution of the star. So keep on twinkling little stars, while I try to figure out what your lithium abundances are.

Contents

Chapter 1

Introduction

4MOST is an abbreviation for the 4-metre Multi-Object Spectroscopic Telescope. This is a fibre fed spectrograph which is to be installed on the 4 metre class VISTA telescope at the Paranal Observatory in Chile. 4MOST will be able to observe 2400 objects at one time and will, by the end of its planned 5 year run, have measured an estimated 20 million spectra in total (De Jong et al. 2019). This will be made possible, in part, by its impressive specifications; a 4.2 square degree field of view, 2436 fibre positioners, one high resolution spectrograph ($\langle R \rangle = 20000$) and two low resolution spectrographs ($\langle R \rangle = 6500$). The development of 4MOST and the planning of its initial observation programme is being carried out by 15 institutes, making up the 4MOST Consortium. The research that is to be done using 4MOST has been categorised into 25 main surveys; 10 prepared by the consortium and 15 prepared by the European Southern Observatory community (Mainieri et al. 2023). The surveys are relevant for many different branches of astrophysics and will provide data that will be useful for both galactic and extragalactic research. One of these branches is the study of stellar evolution. The millions of spectra that will be collected by 4MOST can be used to determine fundamental stellar parameters of the corresponding stars.

The parameter of interest for this project is the lithium abundance within the stellar atmosphere. Its significance, in the context of stellar evolution, is due to lithium being more fragile than other elements found in stellar atmospheres. To put things into perspective, a core temperature exceeding 10 MK is needed to sustain hydrogen fusion and carbon burns at temperatures above 500 MK (Ray 2004). Lithium burns at temperatures as low as 2.5 MK. Its neighbour in the periodic system, beryllium, burns at 3.5 MK and could also be a candidate for probing stellar evolution in similar ways to lithium (Gray 2005). However, absorption lines given by beryllium are only observed in a region in the ultraviolet that is difficult to observe with ground based telescopes (Boesgaard and King 2002). Lithium has an absorption line at 6707.814 Å, hence these wavelengths are easier to detect with ground based telescopes. This, in combination with its fragility, makes lithium a good element to study to gain insight into the evolution of the stars being studied.

How can an elemental abundance give information about a star's evolution? Well, stars are formed within dense regions of gas. This gas is enriched with heavier elements over

time. One example of an event which leads to enrichment of the interstellar medium (ISM) is when a massive star explodes in a supernova at the end of its life, releasing elements it has produced through fusion in its core. The gas becomes more and more enriched and stars being formed in the region will gain a higher initial abundance of these heavier elements. The elemental abundances that a star has at the beginning of its life are therefore affected by the environment in which it is formed, which in turn is affected by time. Due to this, younger stars tend to have higher metallicities than older stars, which were formed out of gas that was less enriched (Jones, Lambourne, and Serjeant 2015).

The elemental abundances will also be affected by certain events in a star's life time. The lithium abundance decreases over the course of a star's life any time that the temperature exceeds 2.5 MK, which it easily does within a star. This has been observed in the Sun, where the lithium abundance has been depleted by a factor of 150 since its birth (López-Valdivia et al. 2015). Certain events have been found to cause a more significant depletion of the lithium abundance. One of these depletion events takes place when a star leaves the main sequence, where it fuses hydrogen into helium, and evolves into a red giant. The transition on to the red giant branch entails that the star undergoes the first dredge up phase. During this phase, the convective layer of the star becomes bigger and reaches further into the star's hotter interior. These deeper regions of the star will not contain any lithium, as temperatures are high enough to destroy it. The lithium in the atmosphere of the star will therefore be diluted as materials from the inner regions are mixed into the convective envelope (Lambert 1981). According to stellar models, this stage of a star's life should destroy the lithium present in its atmosphere. However, 1.2% of red giants are considered to be lithium rich. The origin of these lithium rich stars is not entirely understood. Evidence points to there being a number of different processes of lithium enrichment in red giants. Mass transfer between stars and planetary engulfment are examples of two such processes (Sayeed et al. 2024).

In addition to lithium abundances giving insight into stellar evolution and processes within the stellar interior, they are also valuable to research on galactic evolution and in cosmology. The main isotope of lithium is ^{7}Li and it was produced in significant amounts during Big Bang nucleosynthesis. Theory predicts that ^{6}Li is destroyed in solar-mass stars before they enter the main sequence. If a detectable amount of ^{6}Li is observed, it could be the result of infalling planetary material (Mandell, Ge, and Murray 2004). The amount of ^{7}Li created in the Big Bang is predicted by the standard Big Bang nucleosynthesis(SBBN) theory. Halo stars found on the so called Spite plateau are expected to not have had a depletion of their lithium abundances since they were created (F. Spite and M. Spite 1982). Their lithium abundances should infer the primordial lithium abundance, that is, the abundance of lithium that was created in the Big Bang. The primordial lithium abundance predicted by the SBBN theory is a factor of three lower than what observations of the stars on the Spite plateau infer. This is called the cosmological lithium problem, seeing as the two values do not align. By extension, the validity of the theory behind the values is put into question.

There are multiple sources of lithium enrichment of the ISM, which have caused an increase in its lithium abundance from the primordial value. Even though production processes of ^{7}Li are known to astrophysicists, the enrichment over time within the Milky Way is not completely understood. It is also not completely clear which processes dominate over others (Romano et al. 2021).

Due to the significance of lithium in these areas of astrophysics, accurate and numerous lithium abundance determinations are essential to further our understanding of these aspects of the universe.

1.1 Motivation

This project aims to develop a method for determining lithium elemental abundances for 4MOST, with a similar approach to that presented in the paper titled *3D NLTE Lithium abundances for late-type stars in GALAH DR3* by Wang et al. (2024). At the end of the project, the goal is to be able to determine whether the approach is a good one for 4MOST. A second aim is to be able to compare our results to the results given by the 4MOST pipeline. This would allow us to determine which method performs best.

1.2 Elemental abundances and spectral line strength

As 4MOST has not had first light yet, the spectra that the method will be applied to are synthetic. They have been produced using different input stellar parameters, giving resulting spectra that vary accordingly. For example, a spectrum that has been produced with a higher input metallicity will exhibit stronger iron absorption lines.
The aim is to develop a method that calculates the lithium abundance of a star given its measured spectrum. An elemental abundance is defined as the ratio of the number density of the specified element to the number density of hydrogen present in the stellar atmosphere. The lithium abundance can therefore be expressed as

$$\log A(\mathrm{Li}) = \log\left(\frac{N_{\mathrm{Li}}}{N_{\mathrm{H}}}\right) + 12, \tag{1.1}$$

where N_{Li} and N_H are the number densities of lithium and hydrogen, respectively. Taking the logarithm of the ratio and adding a twelve is standard convention. Another convention for presenting the elemental abundance of a star is to relate it to the corresponding elemental abundance of the Sun. A square bracket notation is used for these values. For example, values for the metallicity ([Fe/H]) and [Li/Fe] are given for each of the synthetic spectra, where

$$[\mathrm{Fe/H}] = \log\left(\frac{N_{\mathrm{Fe}}}{N_{\mathrm{H}}}\right)_\star - \log\left(\frac{N_{\mathrm{Fe}}}{N_{\mathrm{H}}}\right)_\odot = \log A_\star(\mathrm{Fe}) - \log A_\odot(\mathrm{Fe}) \tag{1.2}$$

$$[\mathrm{Li/Fe}] = \log\left(\frac{N_{\mathrm{Li}}}{N_{\mathrm{Fe}}}\right)_\star - \log\left(\frac{N_{\mathrm{Li}}}{N_{\mathrm{Fe}}}\right)_\odot \tag{1.3}$$

In terms of these values, the input lithium abundance for a synthetic spectrum is given by[1]

$$\log A(\mathrm{Li})_{input} = [\mathrm{Fe/H}] + [\mathrm{Li/Fe}] + \log A_{\odot}(\mathrm{Li}). \tag{1.4}$$

The elemental abundance will affect the strength of the absorption lines given by the element in question; a larger amount of absorbers will naturally give rise to more absorption. A measure of the strength of a spectral line is given by the equivalent width, which is defined as

$$W \equiv \int_{\mathrm{line}} \frac{F_c - F_\lambda}{F_c} d\lambda. \tag{1.5}$$

Here, F_λ denotes the flux at wavelength λ and the integral is over the wavelengths that the spectral line covers. Furthermore, F_c is the continuum flux and will be equal to 1 for the synthetic spectra, where the flux has been normalised. The equivalent width is given in units of mÅ. This is because it is equal to the width of a rectangle which has a height of one and has the same area as the spectral line. An illustration of this is shown in figure 1.1, below.

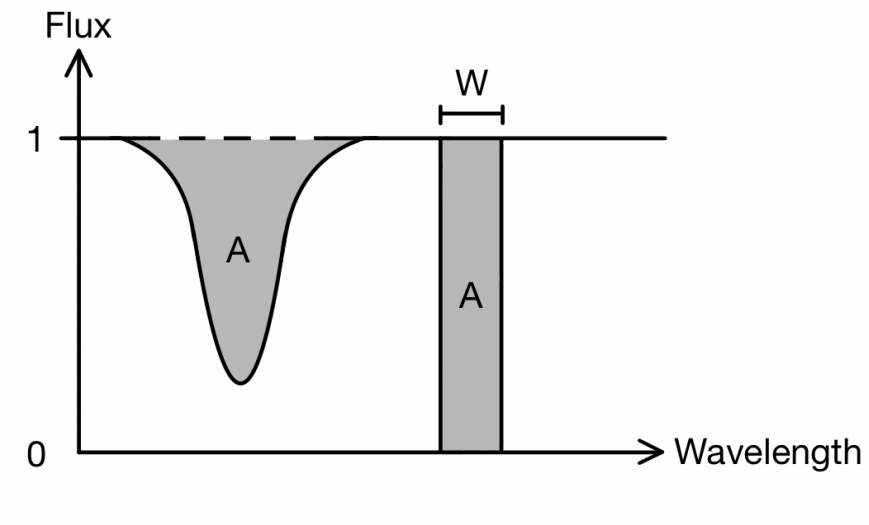

Figure 1.1: Schematic showing how the equivalent width, W, of a spectral line is defined. The areas of the shaded regions are equal and denoted by A.

The rate at which the equivalent width increases with an increased elemental abundance is described by the curve of growth. The curve is given by the logarithm of the equivalent width over the centre wavelength of the line, $\log(W/\lambda)$, as a function of the logarithm of the elemental abundance. All spectral lines have their own curves of growth. To see an example of one, the reader is referred to Figure 13.11 on page 327 in Gray (2005). The curves are affected by different stellar parameters, in ways that are described below. However, there are three regions that are present in all curves of

[1] See Appendix 1 for derivation.

growth. Weak lines have Gaussian profiles and exhibit a linear relationship between $\log(W/\lambda)$ and $\log(A)$. With an increased abundance, the line becomes stronger and eventually it becomes saturated. At this point, the curve of growth plateaus. At higher abundances still, the slope of the curve increases slightly. This is due to the fact that strong lines have a Voigt profile, which is the convolution of a Gaussian and Lorentzian profile. A Lorentzian profile has strong wings, that the Gaussian does not. The strength of these wings increases at this stage of the curve of growth (Gray 2005).

The equivalent width of a spectral line is not only the result of the elemental abundance, it is dependent on other stellar parameters as well. The effective temperature, T_{eff}, is one of these parameters. It controls the extent of excitation and ionization of the absorbers. Assuming that local thermodynamic equilibrium holds, the energy partitioning is given by the local temperature as described by Saha-Boltzmann statistics (Rutten 2003). Given a specific element, or species, the Saha equation gives the ratio of ions to neutral atoms and the Boltzmann equation gives the ratio of atoms excited to a certain level to atoms in a lower level. Both of these distributions are proportional to $\exp(-\chi/kT)$, where χ denotes the excitation or ionization energy and k is Boltzmann's constant. An increase in temperature will give more excitation and ionization, which in turn affect the equivalent width. More excitation events will give a larger equivalent width, seeing as more absorption is taking place. If the species is neutral, ionization will lead to fewer line absorbers. The amount of absorption will decrease as a result, giving a smaller equivalent width. The strength of the absorption line is in this way ruled by the temperature, giving a maximum where the temperature is high enough to give a great extent of excitation and still not high enough to ionize most of the species. Microturbulence, ξ_{micro}, is a stellar parameter describing non-thermal motions in the stellar atmosphere, on the scale of the mean free path of the photon or smaller. A higher microturbulence delays saturation of the spectral line, elongating the linear segment of the curve of growth. Larger equivalent widths are obtained by the lines before they saturate and the curve plateaus.
The surface gravity, denoted by $\log(g)$, is the main stellar parameter that affects the strength of wings of strong lines.

The aforementioned parameters affect the strength of the spectral line. There are processes that do not affect the strength of it, but the shape of it. These are called broadening processes, since they give rise to a broadened line which is wider and shallower. A collection of them are grouped together and called Doppler broadening. This type of broadening arises from motions of thermal and non-thermal origin, on atomic or larger scales. The Doppler width gives the extent of the Doppler broadening and is given by

$$\Delta\lambda_D = \frac{\lambda_0}{c}\sqrt{\frac{2kT}{M} + \xi^2_{micro}}, \tag{1.6}$$

where λ_0 is the centre wavelength of the line and M is the mass of the absorber in kg.

Rotational broadening occurs due to the rotation of the star, with parts of it moving away from us and other parts moving towards us along our line of sight. The result is

a red shift of a portion of the light and a blue shift of another portion of it, resulting in a widened spectral line. This broadening increases with the star's rotational velocity along our line of sight, denoted by $v \sin(i)$.

Chapter 2

Method

In order to obtain the lithium abundance, the goal is to calculate the equivalent width of the Li I line at 6707.814 Å. It is a resonance doublet, meaning that it is made up of two lines given by transitions from the ground state. There are heavier elements that give absorption lines at similar wavelengths, resulting in the lithium line being heavily blended in spectra from stars where these heavier elements are present (Asplund et al. 2009). Molecular CN contributes multiple weak lines across the wavelength region in which the Li I line is found (Mandell, Ge, and Murray 2004).

One can not calculate the equivalent width of the lithium line directly in these spectra, seeing as the observed line is a composite line, the strength of which is contributed to by absorption from multiple species. To calculate the equivalent width of only the lithium line within this blended line, we will make use of information from unblended lines in a wavelength region around the blended line. This approach was taken by Wang et al. (2024). The first step in the process of calculating the equivalent width of the lithium line will be to determine its width. This will be done by making a fit to unblended lines in the wavelength region 6695 - 6720 Å.

The Doppler broadening mentioned above is proportional to the centre wavelength of the line, as well as the square root of the inverse mass of the absorber. This is the only broadening that will vary for the spectral lines. The other processes are governed solely by stellar parameters, which are constant throughout the spectrum. An example of a broadening process that will affect all lines equally is the rotational broadening. The high-resolution spectrograph has a resolution of $R = 18000$ - 21000, which corresponds to a velocity resolution of $\Delta v = 14.3$ - 16.7 km/s via the relation

$$\Delta v = \frac{c}{R}. \tag{2.1}$$

Here, c denotes the speed of light. The Doppler width given in equation (1.6) can be expressed in terms of velocity as

$$\Delta v_D = \sqrt{\frac{2kT}{M} + \xi^2_{micro}}. \tag{2.2}$$

In order to determine whether the resolution of the instrument or the Doppler broadening will dominate the line profile, and hence its width, we consider an extreme case. The maximum microturbulence given for the synthetic spectra is 2.0 km/s, and the maximum temperature is 7998.97 K. The absorber being hydrogen (M $\approx 1.66 \cdot 10^{-27}$ kg) results in a Doppler width of 11.7 km/s. This maximum Doppler broadening is smaller than the width of the instrumental profile. If ^{7}Li is the absorber, the Doppler width is at maximum 4.8 km/s. A conclusion can be drawn that the instrumental profile will be dominating over the Doppler broadening for all lines. The rotational velocities for the synthetic spectra vary from 0.2 m/s to 99.98 km/s. Hence, the rotational broadening will be dominating the width of the spectral lines for velocities that exceed the resolution of the high-resolution spectrograph. The line profiles in the region of interest will therefore be assumed to be dominated by the instrumental profile and rotational broadening.

The unblended lines in the broad region (6695 - 6720 Å) are fitted simultaneously using the Gaussian profile

$$F = 1 - A \cdot \exp\left(-\frac{1}{2}\left(\frac{\lambda - \lambda_0}{\sigma}\right)^2\right), \tag{2.3}$$

where F denotes the flux, A denotes the amplitude of the line and σ denotes the Gaussian width. The parameters of this first fit are the amplitudes of the lines and the Gaussian width of them. All lines in the broad region are assumed to have the same width, seeing as the line profiles are dominated by the instrumental profile and rotational velocity. These are traits that remain the same throughout the region. After obtaining the σ of the lines from the first fit, it is then used as a constant in a second fit. This second fit is made to a narrower region of 6706 - 6710 Å, where the blended line is found. The fit is made to multiple lines in this region, including the lithium line. The σ is fixed for all lines and the parameters of the fit are their amplitudes. The fit is of the same Gaussian shape given in equation (2.3). The resulting amplitude of the lithium line is used together with σ to calculate the equivalent width as

$$W = \sqrt{2\pi} A \sigma. \tag{2.4}$$

Chapter 3

Development on high S/N spectra

3.1 Fitting process

In order to retrieve the equivalent width of the lithium line, a fitting process consisting of the two fits described above was implemented. The first fit was made to the lines listed under Broad Region, in table 3.1. These lines were used by Wang et al. (2024). Two Fe I lines that were used in their study were omitted. These lines are found at 6713.095 Å and 6713.742 Å, respectively. They are too close together for a good fit to be made to each line in 4MOST spectra. The line denoted by V/Ce is made up of a V line and Ce line closely spaced together. The lines denoted by ?1 and ?2 do not have identified species, but were used by Wang et al. (2024) to model an observed feature on the longer wavelength side of the narrow region.

Table 3.1: Centre wavelengths of the lines that the broad and narrow region are applied to, respectively. The corresponding absorbers are listed alongside the centre wavelengths, which are given in Ångström. All lines listed here were used in the study by Wang et al. (2024).

Broad Region (6695 - 6720 Å)	Narrow Region (6706 - 6710 Å)
Al I 6696.085	CN 6706.730
Al I 6698.673	Fe I 6707.433
Fe I 6703.565	CN 6707.545
Fe I 6705.101	Li I 6707.814
Fe I 6710.317	V/Ce 6708.096
Fe I 6711.819	?1 6708.810
Ca I 6717.681	?2 6709.011

The fitting process was first applied to spectra with a signal to noise ratio of 1000 (S/N = 1000). The first spectrum that the fits were made to was given by an approximately solar metallicity, [Fe/H] = 0.05. For this spectrum, the broad region fit is shown in figure 3.1a, below. The lines that the fit was applied to are listed under Broad Region in table 3.1. The resulting Gaussian width of the lines given by this fit is $\sigma = 244 \pm 10$ mÅ. This σ was then fixed for the narrow region fit, which was applied to the lines

listed under Narrow Region in table 3.1. The narrow region fit to the first spectrum, 16101, is seen in figure 3.1b. This fit gave a resulting amplitude of 0.02 ± 0.01 for the lithium line. Using this in equation (2.4) resulted in an equivalent width of 15 ± 9 mÅ.

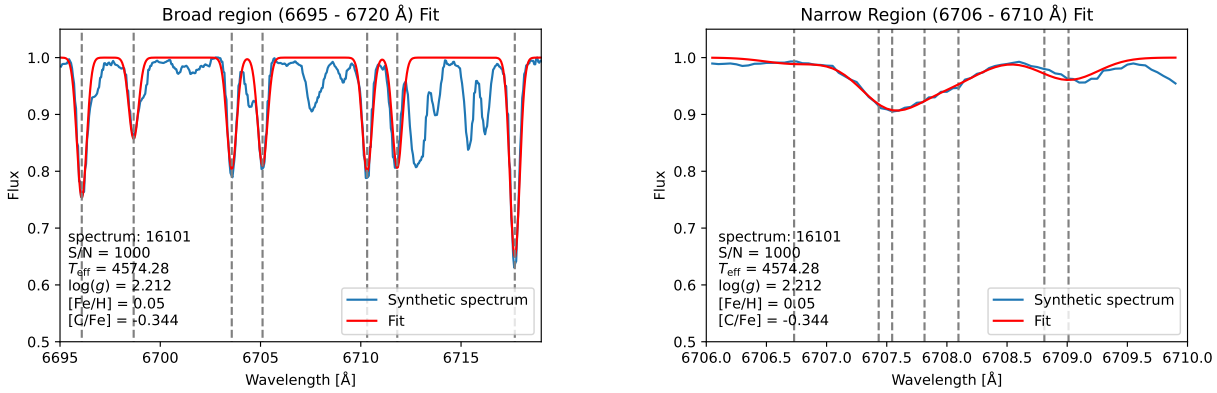

(a) (b)

Figure 3.1: (a) Broad region fit to the spectrum 16101. The effective temperature, surface gravity, metallicity and carbon abundance for this spectrum are listed in the lower left corner of the plot. The vertical grey lines mark the centres of the spectral lines. (b) Fit to the narrow region of spectrum 16101. The vertical grey lines mark the centres of the lines that the narrow region fit is applied to.

Using the obtained width and amplitudes of the lines within the narrow region, the resulting lines could be plotted. They are seen in figure 3.2.

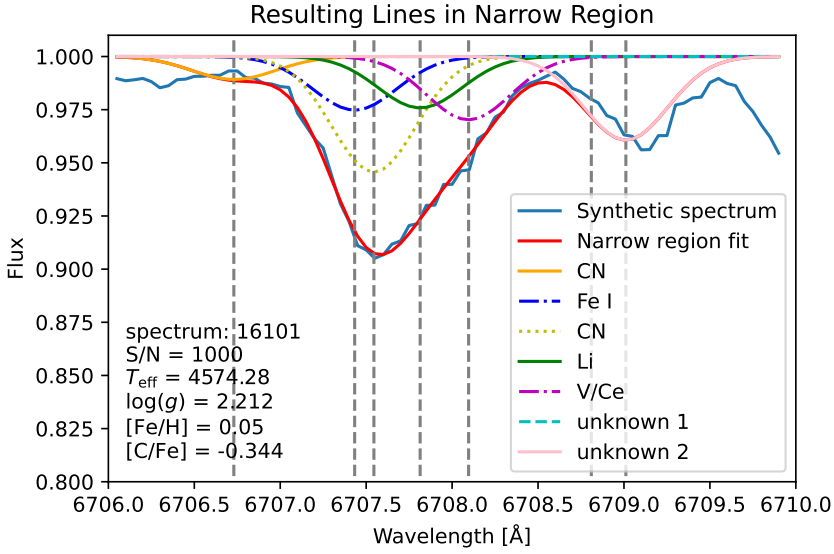

Figure 3.2: Resulting lines, with width given by the broad region fit and amplitudes given by the narrow region fit.

3.2 Application to spectra with S/N = 1000

When the fitting process had been tried on the first spectrum, it was applied to all of the synthetic spectra with S/N = 1000. This was done by iterating through a directory containing the spectra, making the two fits to each of them and saving the resulting σ and W, as well as their corresponding uncertainties. These uncertainties reflect the quality of the fit. In order to gain more insight into which features of the spectrum might be affecting the accuracy of the fit, three conditions were implemented. If any of these conditions are not fulfilled, the resulting fit is considered to be unsuccessful. The three conditions are as follows.

- The flux has to reach the normalised continuum level of $F = 1$. If $F < 0.99$ across the broad region, the spectrum does not fulfil this condition. An example of a spectrum that does not satisfy this condition is spectrum 12617, the broad region fit to which is shown in figure 3.3a. This fit is clearly unsuccessful. The broad region fit made to spectrum 12865 is shown in figure 3.3b. This spectrum has similar stellar parameters to spectrum 12617, bar the carbon abundance, and does fulfil the condition of the flux reaching $F = 1$. These two spectra show why it is important for this condition to be fulfilled in order for a spectrum to be fitted well.

- The number of detected lines in the broad region has to be at least three. Multiple lines present in the broad region is a necessity for measuring an accurate σ. A line is considered to be detected if the following holds for its amplitude given by the broad region fit: $A > 0.5 \cdot \sigma_A$, $\sigma_A \neq 0$ and $A > 0.01$. These thresholds for the amplitude were determined empirically after having tested them on a sample of 15 spectra. If the number of lines detected in the broad region was fewer than three, the condition was not met.

- An upper limit on σ was set to 500 mÅ. This was to ensure that fits giving unreasonably large line widths were identified. Spectrum 12617 is also an example of a case that does not fulfil this condition, with a broad region fit that gives $\sigma = 3320$ mÅ.

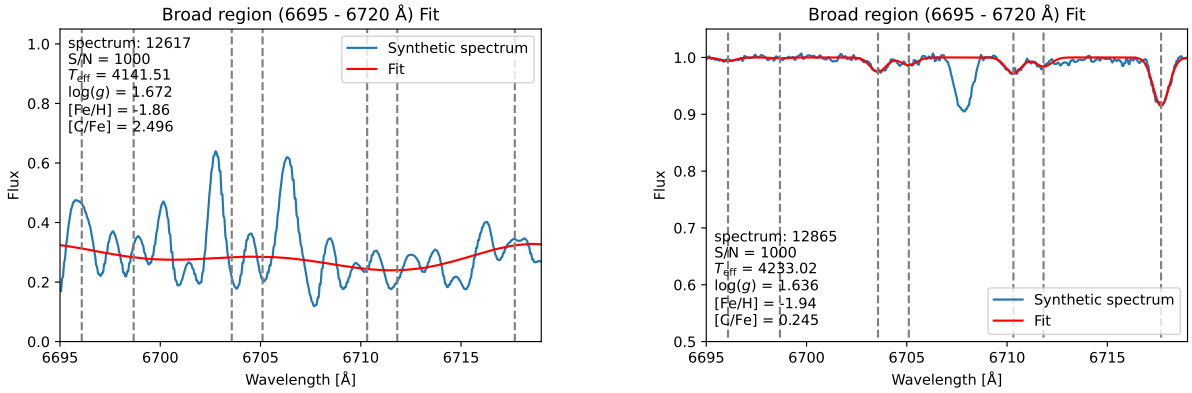

(a) (b)

Figure 3.3: (a) Broad region fit to spectrum 12617, showing an example of a fit that is unsuccessful. (b) Broad region fit to spectrum 12865, which has similar stellar parameters to spectrum 12617, bar [C/Fe].

For the spectra that had fewer than three detected lines in the broad region, a fit was made only to the lithium line. It is assumed not to be blended with other lines in these cases, seeing as a lack of lines in the broad region points to a very low metallicity. This means that the heavier elements giving spectral lines close to the lithium line will have vanishing contributions to the absorption taking place. A detection of lithium in a spectrum that had fewer than three lines in the broad region was defined as the flux in the narrow region being below 0.97 for a tenth of the length of the narrow region. This threshold was determined empirically. In the case of detection, a fit with a Gaussian profile given by equation (2.3) was applied to the lithium line.

Importantly, spectra are discarded after the fitting process if any of the following holds. The flux does not reach $F > 0.99$ at any point across the broad region. The broad region fit fails due to fewer than three lines detected and there is not lithium line detected. The fit applied, either to the broad region or only to the lithium line, gives $\sigma > 0.5$ Å.

Once the procedure described above had been applied to all of the 12704 spectra with S/N = 1000, the Gaussian widths given by successful fits were plotted as a function of $v \sin(i)$. This plot is shown in figure 3.4. The blue dots are given by the broad region fit, and the red dots are given by the fit made directly and only to the lithium line.

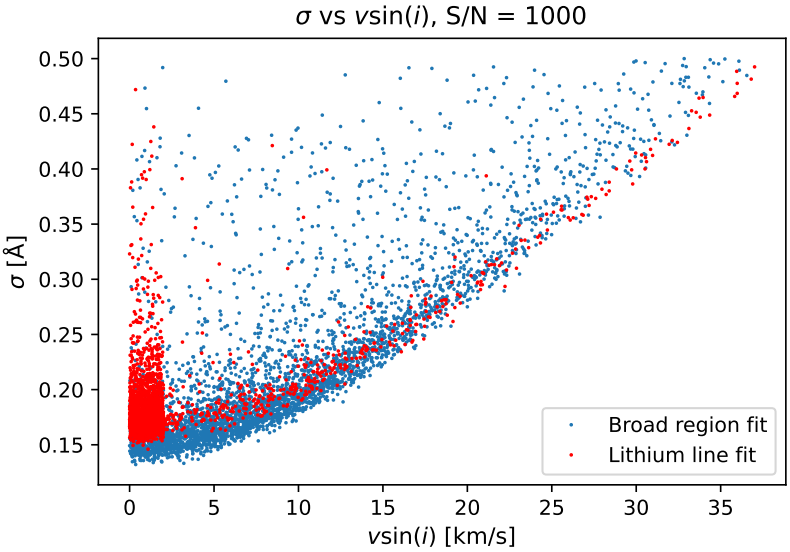

Figure 3.4: The Gaussian widths as a function of rotational velocity along our line of site. The blue points are given by the broad region fit method, and the red points are given by the fit applied only to the lithium line.

The Gaussian width is expected to grow approximately linearly with an increased rotational velocity. This is observed for a set of the Gaussian width in the plot, beyond a rotational velocity of approximately 7.5 km/s. The Gaussian widths that are found above this feature are most likely the result of fits that are not good. Inspecting the broad region fits that give $\sigma > 0.4$ Å for $v\sin(i) < 5$ km/s suggests this is the case. This is elaborated on in the discussion. In order to filter out the unsuccessful fits still remaining after the conditions that were implemented, these bigger Gaussian widths given by the broad region fit are discarded (from the rest of the analysis). To separate these Gaussian widths from the ones that are found in the main linear feature of the plot, the distribution of σ per $v\sin(i)$ is analysed in bins of 2.5 km/s. Gaussians are fit to the distributions and an upper limit for σ is calculated as $\sigma_{max} = \mu_{dist} + 2 \cdot \sigma_{dist}$, for each $v\sin(i)$ bin. Here μ_{dist} denotes the centre of the Gaussian fitted to the distribution of σ, and σ_{dist} denotes the width of it. For $v\sin(i) > 17.5$, km/s the distributions of σ are too spread out to apply a valid Gaussian fit to them. The maximum σ for these higher rotational velocities is determined by making a linear extrapolation from the maximum σ calculated for the four preceding bins of the rotational velocity.
The resulting upper limit for σ, per $v\sin(i)$ bin, was also applied to the data given by the fits made only to the lithium line. An exception was made for $v\sin(i) < 2.5$ km/s, where no upper limit was set for the σ given by the lithium line fit(that is, in addition to the already implemented upper limit of 0.5 Å). The feature that is observed in this region will be discussed later on.

Assuming that data given by unsuccessful fits has now been identified, this data is omitted from the analysis that follows. Equivalent widths that had errors bigger than the calculated value of $W(\mathrm{Li})$ were also omitted from this next step. Using the re-

sulting equivalent widths, $\log(W(\mathrm{Li})/\lambda)$ was plotted as a function of the input lithium abundance. The input lithium abundance is the lithium abundance that was used to produce the synthetic spectrum, and it was calculated using equation (1.4). Colouring the plot by effective temperature showed a clear temperature dependence for the relationship between $\log(W(\mathrm{Li})/\lambda)$ and $\log(A(\mathrm{Li})_{\mathrm{input}})$. This is seen in figure 3.5, below. A lower limit on $\log(W(\mathrm{Li})/\lambda)$ was set to -6, seeing as a signal is indistinguishable from noise below this.

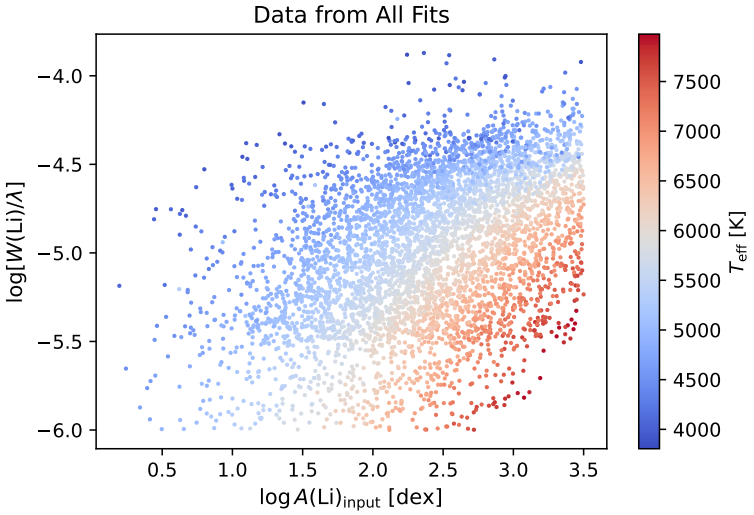

Figure 3.5: Plot of $\log(W(\mathrm{Li})/\lambda)$ vs $\log A(\mathrm{Li})_{\mathrm{input}}$ using data from all successful fits to spectra with S/N = 1000, coloured by T_{eff}.

In order to retrieve $\log A(\mathrm{Li})$ as a function of $W(\mathrm{Li})$ and T_{eff}, we want to fit this data in intervals of T_{eff}. Before doing so, the data was plotted as above but with the logarithm taken of the x-axis. That is, $\log(W(\mathrm{Li})/\lambda)$ was plotted versus $\log(\log A(\mathrm{Li})_{\mathrm{input}})$. (This plot is shown in figure 8.1 in Appendix 2.) The data could be fitted using linear fits in T_{eff} intervals of 150 K. These fits gave slopes and intercepts which were plotted, respectively, versus the centres of the intervals. Linear fits were made to both the slopes and intercepts as functions of T_{eff}. This was done to interpolate the data and be able to retrieve a slope, $a(T_{\mathrm{eff}})$, and intercept, $b(T_{\mathrm{eff}})$, given an effective temperature. Having determined $W(\mathrm{Li})$, $a(T_{\mathrm{eff}})$ and $b(T_{\mathrm{eff}})$, solving for $\log A(\mathrm{Li})$ is now possible.

$$\log[W(\mathrm{Li})/\lambda] = a(T_{\mathrm{eff}}) \cdot \log(\log A(\mathrm{Li})) + b(T_{\mathrm{eff}}) \iff \log A(\mathrm{Li}) = 10^{\frac{\log[W(\mathrm{Li})/\lambda] - b(T_{\mathrm{eff}})}{a(T_{\mathrm{eff}})}}. \quad (3.1)$$

Now, $a(T_{\mathrm{eff}})$ and $b(T_{\mathrm{eff}})$ can be used to calculate lithium abundances when applying the method to the spectra with lower signal to noise ratio.

Chapter 4

Application to spectra with S/N = 100

For the spectra with S/N = 100, a couple of the conditions implemented in the fitting process for spectra with S/N = 1000 needed to be adjusted. This was due to the signal not being as easily distinguished from the noise, and therefore not being detected to the same extent. A line in the broad region was now considered to be present if its amplitude given by the broad region fit fulfilled $A > 0.5$ and $A > 0.5 \cdot \sigma_A$, $\sigma_A \neq 0$. For spectra with fewer than three lines in the broad region, lithium was now considered to be detected if the flux in the narrow region was below 0.95 for at least a fifth of the length of the narrow region. The upper limit for σ remained the same, at 0.5 Å. The check for the spectrum reaching $F > 0.99$ in the broad region remained the same as well.
The changes made were implemented empirically, using the σ vs $v \sin(i)$ plot as a guide. In figure 4.1a and 4.1b, this plot is shown without and with these changes implemented, respectively.

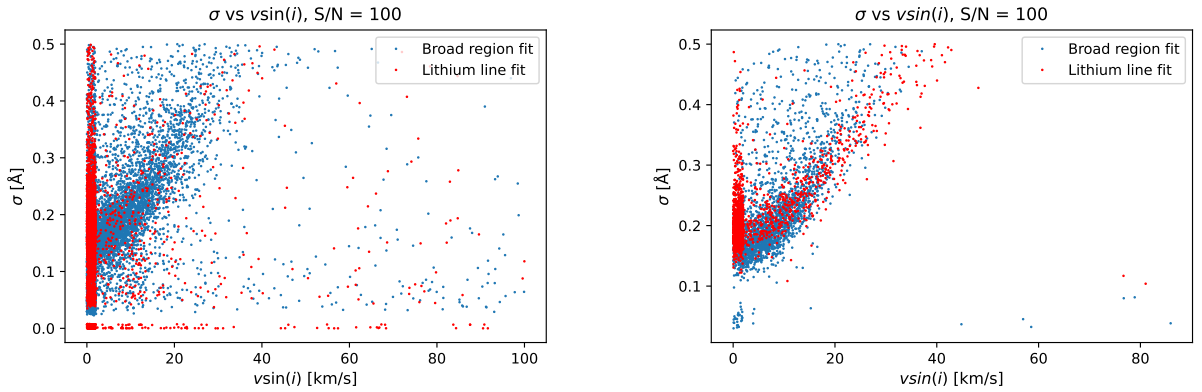

(a) (b)

Figure 4.1: (a) σ vs $v \sin(i)$ plot given by applying the fitting process developed for spectra with S/N = 1000, to spectra with S/N = 100, without making any changes to the conditions necessary for a successful fit. (b) The corresponding plot after having made the changes to the conditions.

Spectra for which the fitting process gave a $\sigma < 0.12$ Å were omitted from the rest of

the analysis as well. This was to make sure that unreasonably small Gaussian widths, observed in figure 4.1b, were discarded. These smaller values for σ were given by fits that managed to pass the check for three peaks in the broad region but were still fitting to the noise and not detected peaks. An example of such a fit is shown in figure 4.2, below.

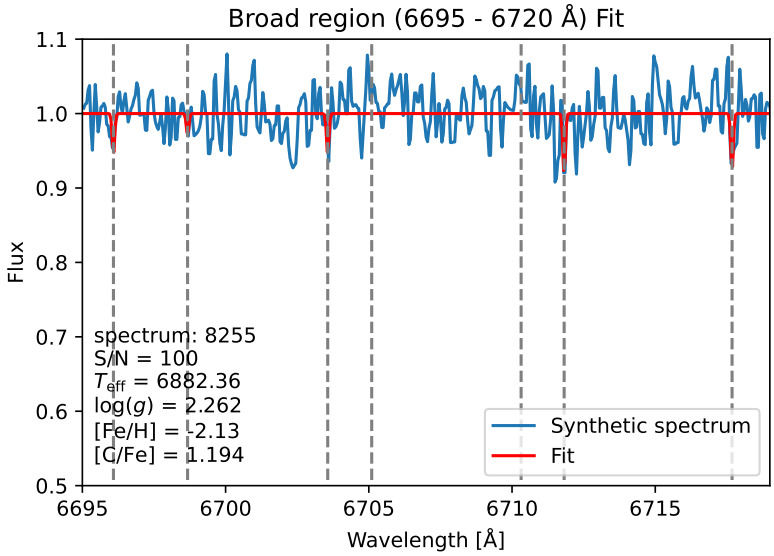

Figure 4.2: Broad region fit to spectrum 8255. This is an example of a fit that fulfilled the condition of having more then three peaks detected, while fitting to noise. The lower limit for σ was implemented to identify this type of unsuccessful fit.

The same process as for the spectra with S/N = 1000 was performed to find an upper limit for σ per $v \sin(i)$. For the spectra that gave a σ below this upper limit, the lithium abundances were calculated using equation (3.1). For $v \sin(i) < 2.5$ km/s, $\log A(\mathrm{Li})$ was calculated for all of the spectra to which the lithium line fit was applied.

Chapter 5

Results

5.1 Spectra with S/N = 1000

Out of the 12704 spectra, with S/N = 1000, that the fitting process was applied to, 3864 fulfilled all three conditions necessary for a successful broad region fit. 7012 spectra had less than three lines in the broad region. Lithium was detected in 3324 of these spectra, 3233 of which gave a $\sigma < 0.5$ Å and had flux reaching $F = 1$. A total of 7097 spectra therefore made it through the fitting process successfully. The resulting σ for the lithium line was plotted as a function of $v \sin(i)$. Figure 5.1 shows the data points that were omitted after having implemented the upper limit for σ as a function of $v \sin(i)$.

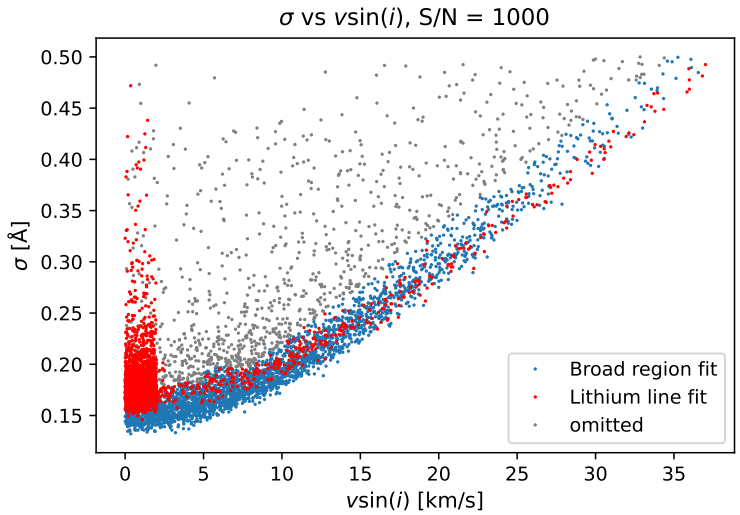

Figure 5.1: The grey points denote data that was discarded. Based on investigations of the fits that have given these data points, the corresponding values of σ are likely the result of an unsuccessful fit.

After this, 6136 spectra had successfully passed all of the aforementioned steps of the analysis. Using the equivalent widths that had errors smaller than the calculated

equivalent width itself, $\log[W(\mathrm{Li})/\lambda]$ vs $\log(\log A(\mathrm{Li}))$ was plotted. The results given by the broad and narrow region fits are shown to the left and the results given by the lithium line fit are shown to the right. Both plots are coloured by T_{eff}. These two sets of data were combined and linear fits were performed to 150 K intervals of T_{eff}.

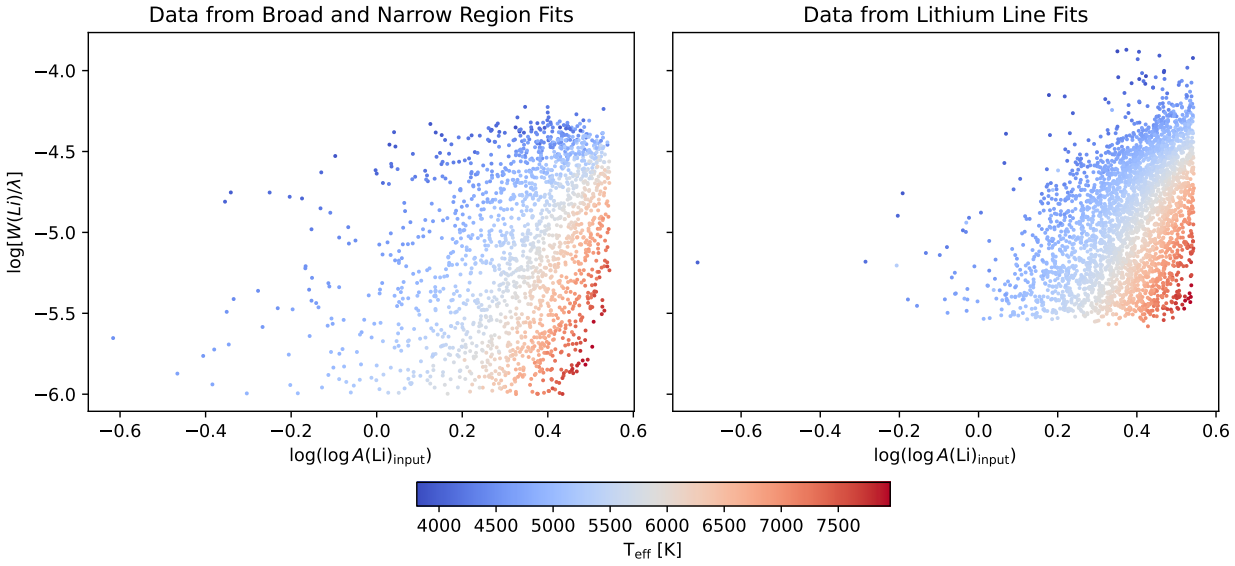

Figure 5.2: Equivalent widths of the lithium line given by the broad and narrow region fit gives the $\log(W(\mathrm{Li})/\lambda)$ vs $\log(\log A(\mathrm{Li})_{\mathrm{input}})$ plot to the left. The equivalent widths given by the fits made only to the lithium line, give the corresponding plot to the right.

The resulting slopes and intercepts of these fits are seen in figure 5.3a and 5.3b, respectively. Linear fits to them allowed for retrieving the slope, $a(T_{\mathrm{eff}})$ and intercept, $b(T_{\mathrm{eff}})$, as functions of T_{eff}.

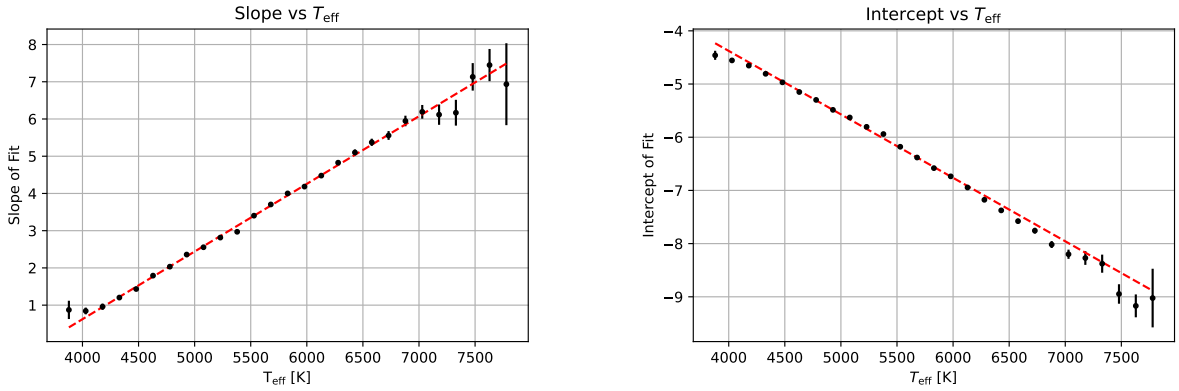

(a) (b)

Figure 5.3: (a) Slope of the linear fits made to $\log[W(\text{Li})/\lambda]$ vs $\log(\log[A(\text{Li})])$, per 150 K interval of T_{eff}, plotted vs the centre T_{eff} of these intervals. Shown in red is the fit made to these points, giving $a(T_{\text{eff}})$. (b) Intercept of the linear fits to $\log[W(\text{Li})/\lambda]$ vs $\log(\log[A(\text{Li})])$, per 150 K interval of T_{eff}, plotted vs the centre T_{eff} of these intervals. The fit made to these points is shown in red, giving $b(T_{\text{eff}})$.

The resulting slope of $\log[W(\text{Li})/\lambda]$ vs $\log(\log[A(\text{Li})])$, as a function of T_{eff} is

$$a(T_{\text{eff}}) = (0.00181 \pm 0.00002) \cdot T_{\text{eff}} - (6.6 \pm 0.1) \tag{5.1}$$

The resulting intercept of $\log[W(\text{Li})/\lambda]$ vs $\log(\log[A(\text{Li})])$, as a function of T_{eff} is

$$b(T_{\text{eff}}) = -(0.00119 \pm 0.00002) \cdot T_{\text{eff}} + (0.38 \pm 0.08). \tag{5.2}$$

5.2 Spectra with S/N = 100

Applying the method to the 12704 spectra with S/N = 100, after having changed the conditions needed to be fulfilled for a good fit, resulted in a successful broad region fit to 2340 spectra. 9015 spectra had fewer than three lines detected in the broad region. Out of these spectra, lithium was detected in 1988. 1718 of these spectra fulfilled the condition of the flux reaching $F = 1$ and had a $\sigma < 0.5$ Å. This means a total of 4058 spectra were considered to have made it through the fitting process successfully.
Figures 3.3a and 3.3b indicate that a higher carbon abundance could be the reason behind unsuccessful fits, in cases where $F < 0.99$ across the broad region and $\sigma > 0.5$ Å. To investigate this further, the input carbon abundance was calculated and the plot shown below in figure 5.4 was made. This suggests that a higher carbon abundance does inhibit successful fits to be to spectra wih lower effective temperatures.

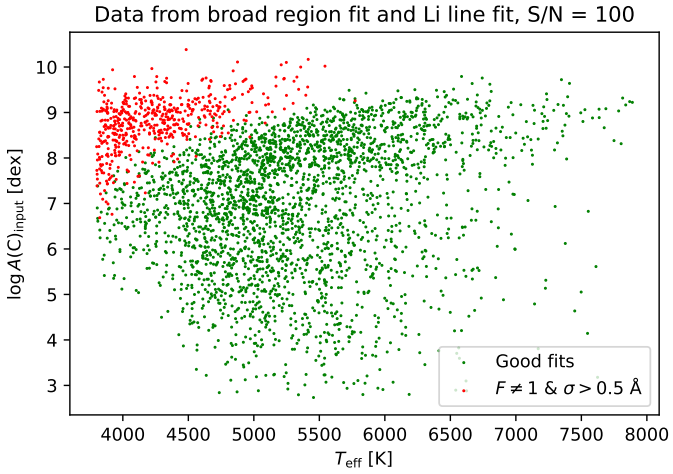

Figure 5.4: Scatter plot showing data from successful fits and fits made to spectra where the flux does not reach 1, resulting in $\sigma > 0.5$ Å, with $\log A(\mathrm{C})_{\mathrm{input}}$ on the y-axis and T_{eff} on the x-axis.

After setting a lower limit of $\sigma = 0.12$ Å and calculating an upper limit for σ per $v\sin(i)$, the resulting plot of σ vs $v\sin(i)$ is shown in figure 5.5

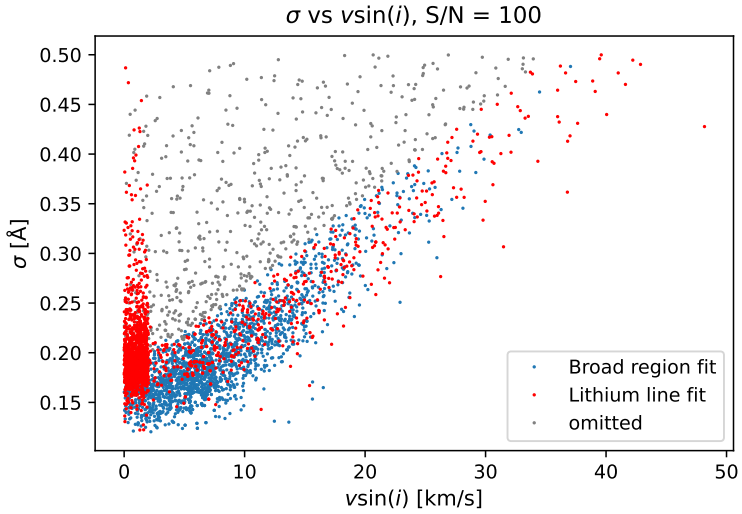

Figure 5.5: Resulting σ vs $v\sin(i)$ plot for spectra with S/N = 100, where grey points denote the data that was omitted from further analysis.

Spectra giving equivalent widths smaller than the uncertainty of the equivalent width were also omitted from further analysis. After this, 2775 spectra were remaining. The calculated $W(\mathrm{Li})$ for these spectra, as well as $a(T_{\mathrm{eff}})$ and $b(T_{\mathrm{eff}})$ derived using spectra with S/N = 1000, were used in equation (3.1) in order to calculate $\log A(\mathrm{Li})$. The logarithm of the absolute difference between the calculated $\log A(\mathrm{Li})$ and $\log A(\mathrm{Li})_{\mathrm{input}}$ is on the x-axis of the histogram shown below in figure 5.6. The number of spectra

giving the corresponding absolute difference is shown on the y-axis. Both spectra with S/N = 100 and S/N = 1000 are included in the histogram. For high resolution spectra with S/N = 100, 4MOST requires that the calculated value of $\log A(\mathrm{Li})$ does not vary with more than 0.2 dex from $\log A(\mathrm{Li})_{\mathrm{input}}$ (Kordopatis et al. n.d.). This is achieved for 2000 of the remaining S/N = 100 spectra. A difference of 0.2 dex corresponds to a value of approximately -0.7 on the x-axis of the plot below.

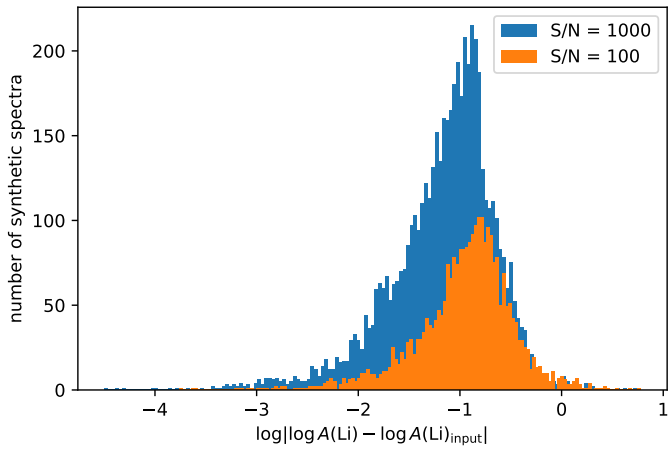

Figure 5.6: Histogram showing the amount of synthetic spectra in bins of the logarithm of the absolute difference between the calculated $\log A(\mathrm{Li})$ and $\log A(\mathrm{Li})_{\mathrm{input}}$.

The following $\log(g)$ vs T_{eff} diagrams show how well our method recovers $\log A(\mathrm{Li})$ for different parts of the diagram, as well as for different metallicities. Figures 5.7a, 5.7c and 5.7e include all spectra in the corresponding metallicity ranges. Figures 5.7b, 5.7d and 5.7f only include the spectra in the same metallicity ranges that have passed all steps of the analysis. The pie charts, per $\log(g)$ and T_{eff} bin, show fractions with colours that represent the following. Red: spectra to which the fit did not make it to the final stage of the analysis. That is, fits that have been categorised as unsuccessful. Orange: spectra to which the fit is considered to have been successful, but the calculated $\log A(\mathrm{Li})$ differs from $\log A(\mathrm{Li})_{\mathrm{input}}$ with more than 0.2 dex. Green: spectra to which a successful fit has been made, resulting in a $\log A(\mathrm{Li})$ that differs with less than 0.2 dex from $\log A(\mathrm{Li})_{\mathrm{input}}$. The diagrams in which squares of different colours are displayed per bin, include the spectra making up the green and orange fractions of the corresponding pie charts. The squares are coloured by the fraction of spectra for which the lithium abundance has been recovered to within 0.2 dex. That is, they represent the percentage of spectra that are green, out of the spectra belonging to green or orange in the pie chart.

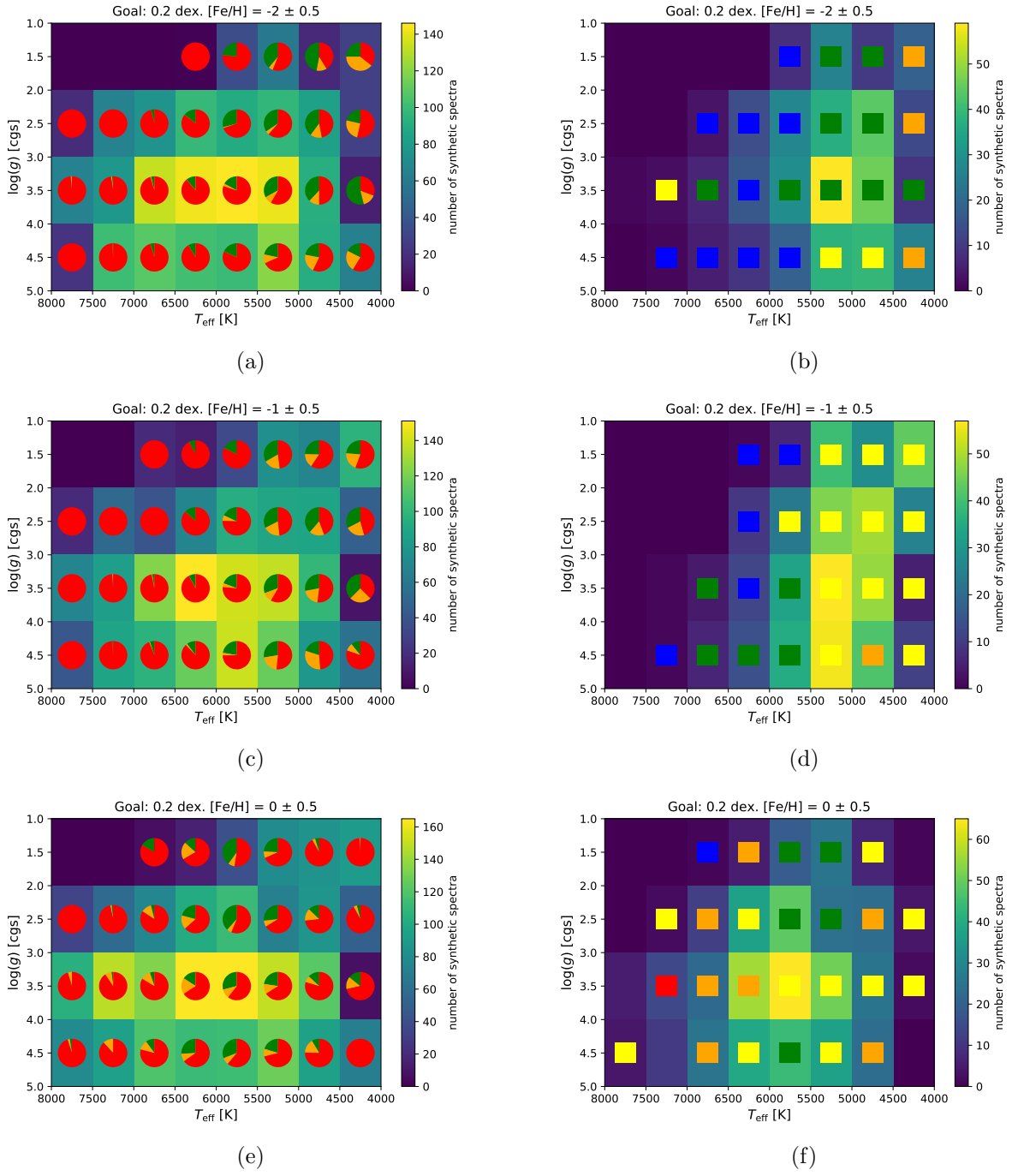

Figure 5.7: Diagrams of $\log(g)$ vs $T_{\rm eff}$ with varying metallicities. (a, c, e) The background of each bin is coloured by the total number of synthetic spectra in it and the colours of the pie charts show how well the fits to the spectra in the bin turned out. Red: unsuccessful fit. Orange: good fit but the recovery of $\log A(\mathrm{Li})$ is not within 0.2 dex. Green: good fit, which gives a recovery to within 0.2 dex. (b, d, f) The background of each bin is coloured by the amount of synthetic spectra in it, to which a good fit is considered to have been made. The squares in each bin represent the fraction of the good fits that result in $|\log(A(\mathrm{Li})) - \log(A(\mathrm{Li})_{\rm input})| < 0.2$ dex. The colours are defined as follows: $> 90\%$ = blue, $75 - 90\%$ = green, $50 - 75\%$ = yellow, $25 - 50\%$ = orange and $< 25\%$ = red.

Chapter 6

Discussion

6.1 Fitting process

The broad and narrow region fitting process is only applicable to spectra with a sufficiently high metallicity, otherwise there would not be three or more lines to apply the broad region fit to. The line list used for the broad region fit seems to have been a good choice. All of the lines are present in spectrum 16101, shown in figure 3.1a, and the line centres shown in grey align well with the observed lines in the synthetic spectrum. As stated, the broad region fit fails if there are fewer than three of these lines present in the spectrum. It has also been found to fail in other scenarios. The first of which is at low temperatures, for spectra with high carbon abundances. This is seen in figure 5.4. A higher carbon abundance brings with it a higher abundance of CN molecules. More absorption by these molecules causes the spectra to look like spectrum 12617, shown in figure 3.3a. Figure 3.3b shows the broad region fit to spectrum 12865. It has similar stellar parameters to spectrum 12617, except for a much lower value of [C/Fe]. The two spectra look very different, with a successful fit being able to be made to one of them and not the other. For spectra in which there is a lot of absorption due to molecular CN, over the wavelength region of interest, one might be better off using other lithium lines to determine the abundance. These lines will not be as strong as the resonance doublet, but they might not be obscured by molecular absorption, giving the opportunity to measure the equivalent width of them.
Another scenario, in which the broad region fit is not good, was identified when investigating the fits giving σ values that were higher than the upper limit set using the σ vs $v\sin(i)$ plot. An example of such a fit is shown in figure 8.2, in Appendix 3. These spectra are very rich in features and the fit is not isolated to the lines of interest. That is, features other than the lines of the broad region line list are fitted to and the result is a wider Gaussian width. A possible solution to this problem could be to apply the fit to one line at a time, and then take an average of the calculated σ. This average σ could then be used in the narrow region fit.

As for the narrow region fit, the line list used could most likely be improved to better suit the synthetic spectra we are applying the fit to. The lines making up the blended line, in which the lithium line is found, seem to model the blended line well. This is

seen in figure 3.2, where the narrow region fit to the blended line looks good. The CN line centred at 6706.730 Å seems to be fitted to quite well in most spectra. The two unknown lines centred at 6708.810 and 6709.011 Å, respectively, do not model the feature found at these wavelengths well. The feature that is observed on the longer wavelength side of the blended line, has its deepest point at a slightly longer wavelength than 6709.011 Å. This is seen in figure 3.1a. The study by Wang et al. (2024), used spectra from stars in the GALAH DR3 catalogue. We are using 1D NLTE synthetic spectra that were produced using line lists comprised with atomic and molecular data, one of which is the Gaia-ESO line list. Using lists such as the Gaia-ESO line list to create synthetic spectra will not result in any prominent unknown lines, which are observed in multiple spectra. At the beginning of this project, a more accurate line list for the narrow region could have been chosen; favourably using the line list used to produce the synthetic spectra as the main source for it. The blended line containing the lithium line is fitted well using the line list we have used, so the calculated equivalent width should not be affected too much by this.

For spectra with lower metallicities, where fewer than three lines in the broad region were detected, a Gaussian fit was made directly to the lithium line. A check for absorption within the narrow region was implemented as a means to identify lithium detection in these spectra. For spectra with S/N = 1000, 3688 spectra had no lithium detected. 7027 of the spectra with S/N = 100 had no lithium detection. One could attribute this large amount of spectra with no lithium detection to the fragility of lithium. If the lithium abundance of the Sun has been depleted by a factor 150 since its creation, it would make sense for stars in our sample with similar, or much higher, T_{eff} to have significantly depleted lithium abundances too. However, we must consider the fact that our 4MOST spectra are synthetic. The lithium abundances that have been assigned to the spectra range from 0 - 3.5 dex and have been distributed quite uniformly with temperature. Meaning that even the spectra with high T_{eff} will have been assigned higher lithium abundances. In figure 3.5 we see that for effective temperatures over 7500 K, lithium abundances lower than 2.5 dex are not detected. This is due to the fact that the equivalent width given by smaller abundances are not distinguishable from the noise. For the spectra with S/N = 100, the smallest equivalent width distinguishable will increase by an order of magnitude, corresponding to a value of $\log[W(\text{Li})/\lambda] = -5$. This means that even fewer spectra with higher T_{eff} will give detections, despite the fact that they too will have been assigned lower abundances.

In figure 5.2, we observe that the lithium line fits do not give as small equivalent widths as the broad and narrow region fit method does. This is most likely the result of the implemented check for lithium detection before a lithium line fit is applied. The broad and narrow region fit is applied for high enough metallicities, regardless of how much absorption is caused by lithium. This means that this method will be able to measure more subtle lithium contributions to the absorption within the narrow region.

Colouring the σ vs $v\sin(i)$ plots by T_{eff} shows that the feature given by the lithium line fits for $v\sin(i) < 2.5$ km/s is made up of fits to cooler spectra. See figure 8.3 in

Appendix 4. Investigating a sample of the fits giving higher values of σ within this feature, confirms that they are given by strong lithium lines. We know that synthetic spectra contributing to the feature are cool and have low metallicity. Lower metallicity stars are often older, as touched on in the introduction. Older stars have been found to rotate with smaller velocities than their younger counterparts (Gruner, Barnes, and Weingrill 2023). 4MOST spectra with [Fe/H] < -2 have therefore been assigned a lower rotational velocity, between 0 and 2.5 km/s (Kordopatis et al. n.d.). The metallicity of the synthetic spectra cover the range of - 5 < [Fe/H] < 0.5. This explains the accumulation of data points from lithium line fits at lower rotational velocities, which has a distinct end at 2.5 km/s.

6.2 Curve of growth

When it came to getting from an equivalent width to an abundance of lithium, we used the curve of growth. Plotting $\log(W(\mathrm{Li})/\lambda)$ vs $\log A(\mathrm{Li})_{\mathrm{input}}$ gave the plot shown in figure 3.5. The relationship between the two values is observed to have a clear temperature dependence. ^{7}Li has an ionisation energy of approximately 5.39 eV, which is quite low. Li I is therefore a minority species. A higher effective temperature results in more ionization, which entails fewer absorbers in the form of Li I. This means that a higher abundance of lithium is needed at higher temperature to obtain the same equivalent width which is achieved by a lower abundance at lower temperatures. This is what we have observed in our plot. An increase in temperature translates the curve of growth in the positive direction along the $\log A(\mathrm{Li})$- axis. When the data is plotted in this way, this is how the temperature affects the curve.
Plateauing is observed in figure 3.5, especially for cooler effective temperatures. This means that we are not only dealing with weak lines. No increase is observed after the plateau. This is a fault of our method. We are fitting using Gaussian profiles, which works for weak lithium lines. However, when we deal with strong lines, they should be fitted with Voigt profiles to get an accurate measure of the equivalent width, which in these cases is contributed to by larger wings of the line.
Plotting $\log(W(\mathrm{Li})/\lambda)$ vs $\log(\log A(\mathrm{Li})_{\mathrm{input}})$ gave the plot shown in figure 8.1. This allowed for fitting the data using linear fits in bins of T_{eff}. The slope of the linear fit increased linearly with temperature, as is seen in figure 5.3a. The intercept of the fit was also observed to decrease approximately linearly with effective temperature, shown in figure 5.3b. Both the slope and intercept were interpolated linearly as functions of T_{eff}. This means that given an equivalent width and an effective temperature, we can calculate the corresponding lithium abundance. The distribution given by the S/N = 1000 spectra in the histogram shown in 5.6 points to this fitting process not being perfectly accurate. Specifically, the tail that extends in positive direction, beyond -0.7, along the $\log|\log A(\mathrm{Li}) - \log A(\mathrm{Li})_{\mathrm{input}}|$-axis. This inaccuracy most likely stems from the fits made to the data in figures 5.3a and 5.3b not being great towards the lower and higher end of the T_{eff}-axis.

6.3 Performance of method

Out of the 12704 spectra with S/N = 100 that the method was applied to, $\log A(\mathrm{Li})$ was calculated to within 0.2 dex of $\log A(\mathrm{Li})_{\mathrm{input}}$ for 2000 spectra. As discussed above, this small amount of spectra is partly due to lithium not being detected in a vast amount of the spectra. Another contributing factor is the difficulty in determining whether or not a fit has been successful or not. A χ^2 value could not be used as an indicator of a successful fit. This is because we are not fitting all features across the region over which the fit is made. These features will look different depending on many stellar parameters. The calculated χ^2 value can therefore not be used as measure of the accuracy of a fit, seeing as it too will vary depending on these parameters. The σ vs $v\sin(i)$ plot was used to identify spectra that had managed to fulfil the conditions for a successful fit and still did not look good. However, this approach is not very accurate. There could be unsuccessful fits giving data points that happen to fall within the set that we did not omit. Vice versa, there could be good fits present in the data that was omitted. With the high amounts of spectra that we have, and with the much higher amount that will be collected with 4MOST, it is near impossible, or at least very ineffective to check whether individual spectra have been fitted well or not. This means that our filtering process needs to be reliable, which is difficult to guarantee, seeing as the spectra that will be collected will have a vast variety of different characteristics. This has been seen in our study and it has been difficult to implement conditions that have to be met for a fit to be considered successful.

The diagrams in figure 5.7 give more insight into in which cases the method is applicable and works well. For the spectra that made it this far in the analysis, the rate of recovery of $\log A(\mathrm{Li})$ to within 0.2 dex seems quite high. Most squares are yellow or green, which means that $\log A(\mathrm{Li})$ has been successfully calculated for $50-75\%$ or $75-90\%$ of the spectra in these bins. This shows that the method has promise and that this approach to calculating the equivalent width of the lithium line is a good one, as it results in accurately calculated lithium abundances. The diagrams for the higher metallicity ($-0.5 < [\mathrm{Fe/H}] < 0.5$) spectra, in figures 5.7f and 5.7e, point specifically to the promise of the broad and narrow region fit method. For higher metallicity, this method is applicable and allows for the calculation of the equivalent width of the lithium line within the blended line. This results in a slightly better retrieval of the lithium abundances at higher temperatures, as seen in the diagrams. For lower metallicities, the broad and narrow region fit is not applicable to the same extent and a fit is made only to the lithium line, if one is detected. If the lithium abundance is too small to give a detection, a fit is not made. As discussed above, we detect far from the full range of lithium abundances that have been assigned to the synthetic spectra, at higher temperatures in particular. This explains why there are so few spectra present at higher temperatures in diagrams 5.7b, 5.7d and 5.7f. The lower number of spectra in the bins at lower temperatures is most likely due to the molecular CN absorption that was discussed above.

A secondary goal of this study was to be able to compare the results with those given

by the 4MOST pipeline. Similar diagrams to the ones presented in figures 5.7b, 5.7d and 5.7f have been made for the results of the pipeline (Kordopatis et al. n.d.). It is difficult to make a direct comparison of the diagrams, as the sizes of our samples of test spectra are different. The method used to calculate the lithium abundances in the pipeline does not have a process of filtering out spectra where an abundance can not be determined. This also makes it difficult to make a direct comparison of the results by studying the diagrams that have been produced by the two methods. However, the colours of the squares presented in our diagram for $-0.5 < [\mathrm{Fe/H}] < 0.5$, are comparable to the ones presented in the diagram for the same metallicity range from the pipeline. Towards lower metallicity, our method seems to improve and the colours show a higher fraction of recovery to within 0.2 dex. By filtering out cases where a reliable fit is not made, the validity of the calculated lithium abundances is increased.

Chapter 7

Conclusion

The main goal of this project was to develop a method for determining lithium abundances from spectra that are to be collected by 4MOST. This has been done, as we have successfully recovered $\log A(\mathrm{Li})$ to within the 4MOST requirement of 0.2 dex for high resolution spectra with a signal to noise ratio of 100. Our method was applied to 12704 4MOST synthetic spectra, out of which $\log A(\mathrm{Li})$ was recovered to within 0.2 dex for 2000 spectra. This low number is the result of a large amount of unsuccessful determinations of the equivalent width of the Li I line. Some cases where these unsuccessful determinations happen have been identified and can be summarized as follows.

- Non-detections, where the Li I line is too weak to be fitted and an equivalent width can not be determined. The strength of the Li I line has been observed to decrease with effective temperature, so these non-detections are more numerous at higher values of T_{eff}.
- Feature rich spectra, where the broad region fit fails due to fitting over features other than the individual lines that the fit is applied to. This results in a line width that is bigger than it should be.
- Molecular CN absorption hinders successful fitting to the region of interest, for spectra with lower effective temperatures and higher carbon abundances.

Although the lithium abundance is only recovered to within 0.2 dex for 2000 of the spectra, the fact that it has been successfully recovered for them points to the promise of the method. The broad and narrow region fit method was successful in determining the equivalent width of the Li I line in cases where it was heavily blended.
As for our secondary goal, comparing our results to results produced by the 4MOST pipeline indicates that our results are comparable. However, a direct comparison between the two sets of results could not be made.

To improve this method, future research could focus on making it more suitable for application to real, 3D NLTE spectra. When spectra have started to be measured by 4MOST, a more appropriate line list for the region of interest can be constructed. The lithium line can also be fitted using a profile that takes 3D effects into account.

An advantageous feature of our method is that a vast amount of unreliable results are identified and discarded. This feature could potentially be implemented into the pipeline.

Acknowledgements

I would first and 4most like to thank my supervisor Ross Church for his help during my first introduction to research in astrophysics. Thank you for giving me the opportunity to do this project with you. Thank you for the discussions and for being there when I had questions.
Thank you to my friends and colleagues Nellie, Sofia and Ossian for being the best study buddies. Thank you to William for making my days much brighter and for cheering me on every step of the way.

Thank you to Pappa James, Grandpa Keith and Grandma Jennifer for your love and support, which is felt all the way over here in Lund.

To Mormor Marita, Mamma Anna, Erika and Iman, thank you for shaping me into who I am today. Thank you for the love, laughter and lessons. Words are not enough, but thank you for everything.

Bibliography

Asplund, Martin et al. (Sept. 2009). "The Chemical Composition of the Sun". In: *ARA&A* 47.1, pp. 481–522. DOI: 10.1146/annurev.astro.46.060407.145222. arXiv: 0909.0948 [astro-ph.SR].

Boesgaard, Ann Merchant and Jeremy R. King (Jan. 2002). "Beryllium in the Hyades F and G Dwarfs from Keck HIRES Spectra". In: *The Astrophysical Journal* 565.1, p. 587. DOI: 10.1086/324436. URL: https://dx.doi.org/10.1086/324436.

De Jong, Roelof S. et al. (2019). "4MOST: Project overview and information for the First Call for Proposals". In: *Published in The Messenger* vol. 175, pp. 3–11. DOI: 10.18727/0722-6691/5117. URL: https://doi.eso.org/10.18727/0722-6691/5117.

Gray, David F. (2005). *The Observation and Analysis of Stellar Photospheres*. Cambridge University Press.

Gruner, Barnes, and Weingrill (2023). "New insights into the rotational evolution of near-solar age stars from the open cluster M 67". In: *AA* 672, A159. DOI: 10.1051/0004-6361/202345942. URL: https://doi.org/10.1051/0004-6361/202345942.

Jones, Mark H., Robert J. A. Lambourne, and Stephen Serjeant (2015). *An Introduction to Galaxies and Cosmology*. Cambridge University Press.

Kordopatis, G. et al. (n.d.). *The 4MOST galactic pipeline*. in preparation.

Lambert, D. L. (Jan. 1981). "The chemical composition of red giants - The first dredge-up phase". In: *Physical Processes in Red Giants*. Ed. by I. Iben Jr. and A. Renzini. Vol. 88. Astrophysics and Space Science Library, pp. 115–134. DOI: 10.1007/978-94-009-8492-9_10.

López-Valdivia, R. et al. (June 2015). "Lithium abundance in a sample of solar-like stars". In: *Monthly Notices of the Royal Astronomical Society* 451.4, pp. 4368–4374. ISSN: 0035-8711. DOI: 10.1093/mnras/stv1222. eprint: https://academic.oup.com/mnras/article-pdf/451/4/4368/3886893/stv1222.pdf. URL: https://doi.org/10.1093/mnras/stv1222.

Mainieri, V. et al. (Mar. 2023). "The 4MOST Community Surveys". In: *The Messenger* 190, pp. 3–3. DOI: 10.18727/0722-6691/5298.

Mandell, Avi M., Jian Ge, and Norm Murray (Feb. 2004). "A Search for6Li in Lithium-Poor Stars with Planets". In: *The Astronomical Journal* 127.2, pp. 1147–1157. ISSN: 1538-3881. DOI: 10.1086/380944. URL: http://dx.doi.org/10.1086/380944.

Ray, A. (2004). *Stars as thermonuclear reactors: their fuels and ashes*. arXiv: astro-ph/0405568 [astro-ph]. URL: https://arxiv.org/abs/astro-ph/0405568.

Romano et al. (2021). "The Gaia-ESO Survey: Galactic evolution of lithium from iDR6". In: *AA* 653, A72. DOI: 10.1051/0004-6361/202141340. URL: https://doi.org/10.1051/0004-6361/202141340.

Rutten, Robert J. (May 2003). *Radiative Transfer in Stellar Atmospheres*.

Sayeed, Maryum et al. (Mar. 2024). "Many Roads Lead to Lithium: Formation Pathways For Lithium-rich Red Giants". In: *The Astrophysical Journal* 964.1, p. 42. ISSN: 1538-4357. DOI: 10.3847/1538-4357/ad1936. URL: http://dx.doi.org/10.3847/1538-4357/ad1936.

Spite, F. and M. Spite (Nov. 1982). "Abundance of lithium in unevolved stars and old disk stars : Interpretation and consequences." In: *A&A* 115, pp. 357–366.

Wang, Ella Xi et al. (2024). *3D NLTE Lithium abundances for late-type stars in GALAH DR3*. arXiv: 2402.02669 [astro-ph.SR]. URL: https://arxiv.org/abs/2402.02669.

Chapter 8

Appendix

8.1 Appendix 1

$$\log A(\mathrm{Li}) = \log\left(\frac{N_{\mathrm{Li}}}{N_{\mathrm{H}}}\right) + 12 = \log(N_{\mathrm{Li}}) - \log(N_{\mathrm{H}}) + 12 \tag{8.1}$$

$$= \log(N_{\mathrm{Li}}) - \log(N_{\mathrm{H}}) + \log(N_{\mathrm{Fe}}) - \log(N_{\mathrm{Fe}}) \tag{8.2}$$

$$+ \log(N_{\mathrm{Li}}^{\odot}) - \log(N_{\mathrm{Li}}^{\odot}) + \log(N_{\mathrm{Fe}}^{\odot}) - \log(N_{\mathrm{Fe}}^{\odot}) \tag{8.3}$$

$$+ \log(N_{\mathrm{H}}^{\odot}) - \log(N_{\mathrm{H}}^{\odot}) + 12 \tag{8.4}$$

$$= \underbrace{\log(N_{\mathrm{Li}}) - \log(N_{\mathrm{Fe}}) - \log(N_{\mathrm{Li}}^{\odot}) + \log(N_{\mathrm{Fe}}^{\odot})}_{[\mathrm{Li/Fe}]} \tag{8.5}$$

$$+ \underbrace{\log(N_{\mathrm{Fe}}) - \log(N_{\mathrm{H}}) - \log(N_{\mathrm{Fe}}^{\odot}) + \log(N_{\mathrm{H}}^{\odot})}_{[\mathrm{Fe/H}]} \tag{8.6}$$

$$+ \underbrace{\log(N_{\mathrm{Li}}^{\odot}) - \log(N_{\mathrm{H}}^{\odot}) + 12}_{\log A_{\odot}(\mathrm{Li})} \tag{8.7}$$

$$= [\mathrm{Li/Fe}] + [\mathrm{Fe/H}] + \log A_{\odot}(\mathrm{Li}) \tag{8.8}$$

8.2 Appendix 2

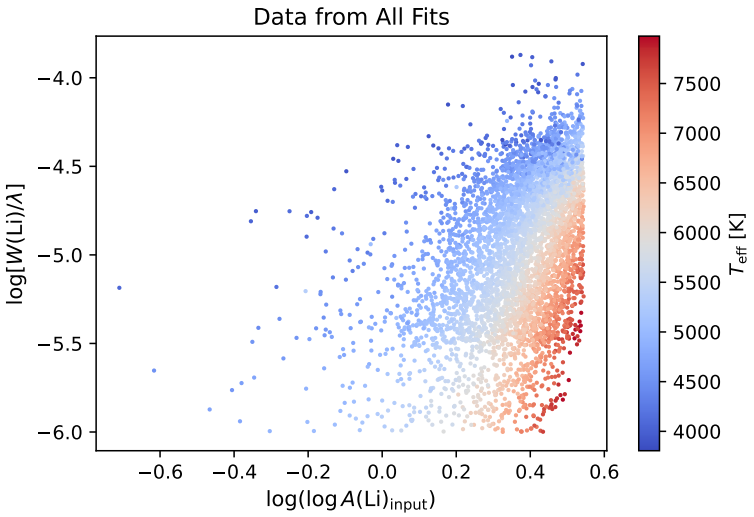

Figure 8.1: Plot of $\log(W(\mathrm{Li})/\lambda)$ vs $\log(\log A(\mathrm{Li})_{\mathrm{input}})$, coloured by T_{eff}.

8.3 Appendix 3

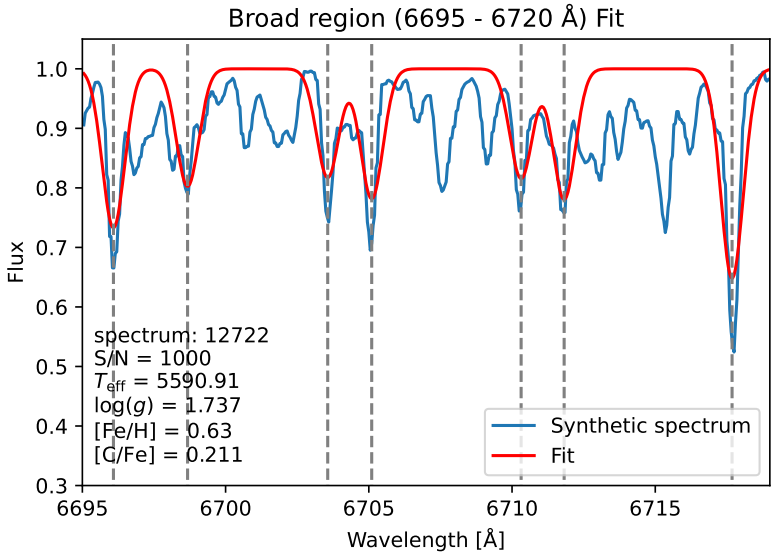

Figure 8.2: Broad region fit to spectrum 12722.

8.4 Appendix 4

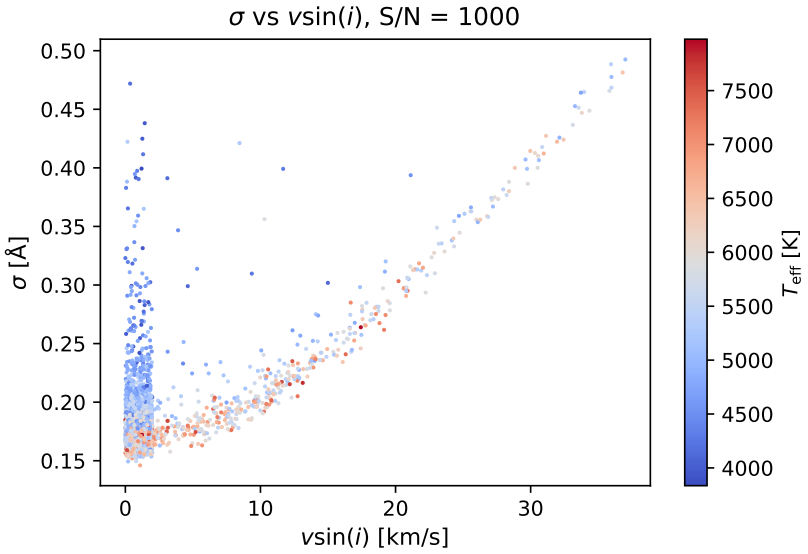

Figure 8.3: σ vs $v\sin(i)$ given by lithium line fits to spectra with S/N = 1000, coloured by T_{eff}.